CGMS-43 IOC-WP-01
2 May 2015

Prepared by IOC-UNESCO
Agenda Item: D.7
Discussed in Plenary

AQUARIUS AND SMOS SEA SURFACE SALINITY MEASUREMENTS: A REVIEW OF INITIAL RESULTS

In response to CGMS Action 42.10
HLPP reference: 1.1.6

Executive Summary

The global water balance and the relative magnitudes of its global and regional components are of fundamental importance to society and are largely unmeasured over the ocean. The advent of satellite sea surface salinity (SSS) measurements by the Soil Moisture and Ocean Salinity (SMOS) mission launched in November 2009 and the Aquarius on the fourth Argentine Satélite de Aplicaciones Cientificas (SAC-D) satellite mission launched in June 2011, respectively, opened a new era in ocean sciences. This paper outlines the new measurement systems, including a preliminary assessment on the technological challenges, and provides an overview of results, including the salt budget in the North Atlantic, tropical instability waves, Rossby waves, mesoscale motions, freshening of surface coastal waters from riverine outflow and impact on hurricane forecasting in northwest Atlantic, and SSS response to La Niña. As the SSS time series lengthen with continued mission operations, SSS data will receive additional attention in numerous studies, including the El Niño/La Niña phenomenon, Gulf Stream meanders, and global salt budget of the water balance.

Recommendation proposed: (1) Support sustained high spatial and high frequency SSS measurements for improved weather and climate applications. (2) Assimilate measurements of satellite SSS, sea surface temperature, and ocean surface topography, together with in-situ measurement, into ocean general circulation models to improve estimates of vertical profiles of ocean currents and ocean heat transport.

AQUARIUS AND SMOS SEA SURFACE SALINITY MEASUREMENTS: A REVIEW OF INITIAL RESULTS

David Halpern[1]
NASA / California Institute of Technology Jet Propulsion Laboratory
Pasadena, CA 91109, USA

Jordi Font
Institut de Ciencies del Mar CSIC
Barcelona 08003, SPAIN

Gary Lagerloef
Earth and Space Research
Seattle, WA 98121, USA

1 INTRODUCTION

Sea surface salinity (SSS) is a fundamental ocean state variable and alters sea surface temperature (SST) through the SSS influence on ocean surface density. Also, SSS is a tracer of ocean circulation and an important component of the global water balance. What makes the study of SSS so fascinating is that a variety of processes occur simultaneously and also occur coincidently with other processes.

The SSS unit is dimensionless because salinity is defined as the weight of salt in grams in 1 kg of seawater. The typical SSS in the global ocean is 35 g $(kg)^{-1}$ or 35 practical salinity units (psu). A SSS increase of 0.2 psu and a decrease of 1 °C in SST would each increase seawater density by approximately the same amount. The SSS has been very undersampled compared to SST because accurate measurements of SSS are difficult to make and the relatively small SSS range of ~ 5 psu requires a higher precision than SST, which has a range of ~ 30°C. The capability of measuring SSS from satellite spawned a renewal in the study of many subjects linked to SSS.

[1] For this paper, David Halpern represents the Intergovernmental Oceanographic Commission (IOC) of the United Nations Educational, Scientific, Cultural Organization (UNESCO), which is a member of the Coordination Group for Meteorological Satellites (CGMS). The World Meteorological Organization (WMO) – IOC Joint Commission on Oceanography and Marine Meteorology (JCOMM) supports IOC to accomplish CGMS Plenary Action 42.10, which invited IOC to provide a paper on guidance to CGMS members on sea surface salinity observations.

2 EVALUATION OF SATELLITE SSS MEASUREMENTS

Two pilot satellite missions dedicated to SSS measurements are on operational orbit using L-band (1-2 GHz) frequency radiometry. Measuring SSS from space is challenging because the sensitivity of a measurement of the microwave radiation traveling upward from the top of the atmosphere to the satellite, which is known as brightness temperature (http://www.remss.com/measurements/brightness-temperature), at L-band frequencies to SSS is weak, about 0.5 K psu^{-1} (Yueh et al., 2001). At L-band frequencies the brightness temperature recorded at the satellite is related to SST and sea surface emissivity, which depends on SSS and other properties such as roughness from surface wind, waves, swell, currents and SST.

The European Space Agency (ESA) Soil Moisture and Ocean Salinity (SMOS) satellite mission was launched on 2 November 2009 (commissioning phase ended in May 2010) and the pre-launch accuracy goal of open ocean SSS was 0.1-0.2 psu averaged for 10-30 days over a 100- to 200-km grid (Font et al., 2010). The United States National Aeronautics and Space Administration (NASA) Aquarius SSS-measuring instrument was launched on the fourth Argentine Satélite de Aplicaciones Cientificas (SAC-D) satellite mission on 10 June 2011 (commissioning phase ended in August 2011) with a pre-launch accuracy goal of 0.2 psu over a 30-day average within an open ocean area of 150 km by 150 km (Lagerloef et al., 2012). The name “Aquarius/SAC-D” will be shortened to “Aquarius”. The Aquarius and SMOS measurement system technologies were different, and both missions represent first-time technological achievements (Lagerloef and Font, 2010). Aquarius has three separate radiometers viewing at 29, 38 and 46 degrees from nadir and a 1.26-Gz scatterometer to estimate corrections for the effects of surface roughness. Meissner et al. (2014) reported that the measured roughness correction reduced the root-mean-square difference (rmsd) of Aquarius SSS measurements by about 40%. SMOS has a two-dimensional interferometric radiometer and uses the European Centre for Medium-range Weather Forecasts operational numerical weather prediction surface wind data product to estimate the surface roughness correction. The Aquarius and SMOS orbit heights are 657 and 756 km, respectively. Aquarius and SMOS equatorial crossing local times are 0600 and 1800 (descending or southward) and 1800 and 0600 (ascending or northward). The Aquarius and SMOS time intervals for global coverage are 7 and 3 days, respectively.

Evaluating the accuracy of a satellite data product is challenging because the satellite, which moves at ~ 7 km s^{-1}, provides a near-instantaneous measurement compared to an in-situ measurement averaged over several minutes to hours. The satellite SSS footprint (76 x 94 km^2, 84x120 km^2 and 96x156 km^2 for Aquarius; 40x40 km^2 for SMOS) is nearly infinitely larger than an in-situ measurement and can display significant SSS variability. Also, a satellite measures salinity in the 1-cm skin of the ocean whereas an in-situ measurement is usually representative of a near-surface depth interval. Thus, SSS measured by satellite and in-situ instrumentation will differ in horizontal, vertical and temporal dimensions.

SSS recorded with Aquarius and SMOS have similar large-scale features (Figures 1a and 1b), which provide opportunities for producing an integrated data product to reduce aliasing caused by inadequate sampling.

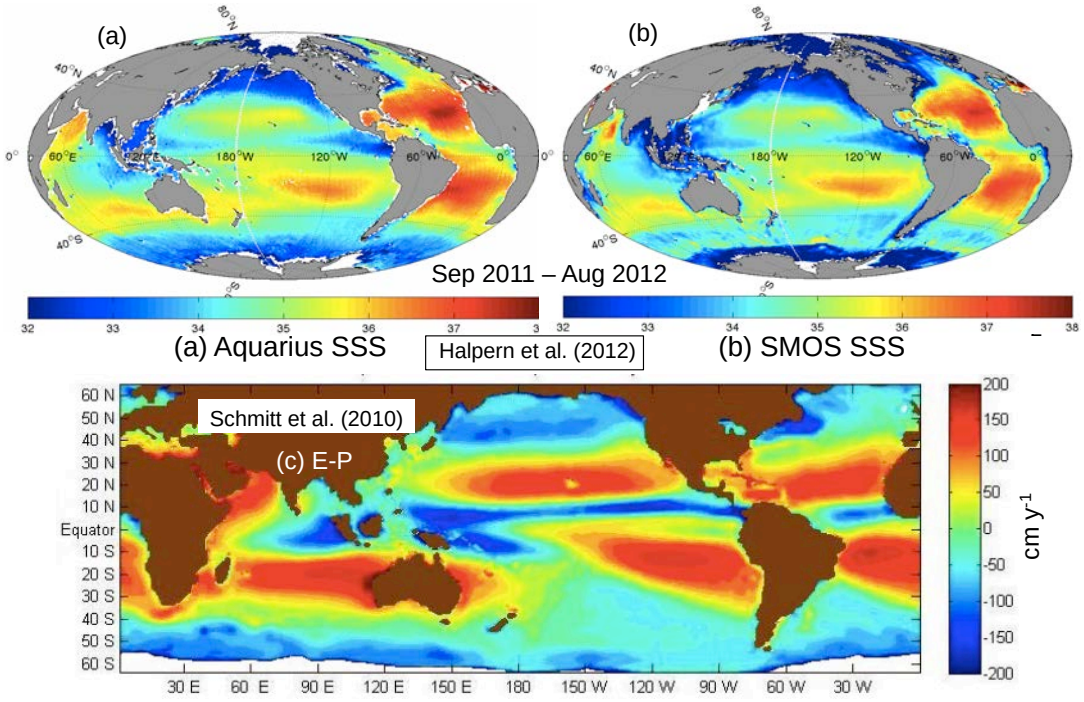

Figure 1. Sea surface salinity measurements recorded in 1 September 2011 – 31 August 2012 with (a) Aquarius and (b) SMOS missions. Units are psu. Diagram extracted from Halpern et al. (2012). (c) Climatological-mean annual average evaporation minus precipitation, based on evaporation estimates by Yu and Weller (2007) and satellite-based precipitation estimates from the Global Precipitation Climatology Program (available at http://precip.gsfc.nasa.gov). Units are cm. Diagram extracted from Schmitt et al. (2010).

2.1 Vertical Salinity Variations

Argo floats, which make the shallowest salinity measurement at 5 m (Riser et al., 2008), provide a global quasi-SSS dataset because the difference in the 1-cm and 5-m depths of the satellite and Argo measurements, respectively, is most of the time smaller than the design goal of Aquarius and SMOS SSS measurements. Drucker and Riser (2014) showed that although rain events identified from the Tropical Rainfall Measuring Mission precipitation measurements produced stratification greater than 0.1 psu, their infrequent occurrence and short duration would contribute a bias less than 0.03 psu in the tropics. Henocq et al. (2010) observed SSS differences greater than ± 0.1 psu between the surface and 5-m depth in about 3% of the extensive database, i.e., 97% of the time the salinity difference between the surface and 5 m was negligible with regards to the design goal of Aquarius and SMOS SSS measurements. A number of comparative studies of Argo and SSS indicate that the accuracies of both Aquarius and SMOS SSS are approaching their pre-launch goals. For example, Boutin et al. (2012) found SMOS rmsd accuracy of 0.3-0.5 psu over a 10-day period and within a 100-km by 100-km region. Abe and

Ebuchi (2014) found Aquarius rmsd accuracy of 0.37 psu for matchup separations less than 200 km and less than 12 h. Note that the rmsd between satellite SSS and near-surface in-situ salinity is influenced by two factors: (1) the vertical difference of salinity between the 1-cm satellite radiometric depth and the 5-m Argo in-situ depth; and (2) the spatial variation of SSS within the satellite footprint, which is not represented by in-situ measurements and which is discussed in the next section.

2.2 Horizontal SSS Variations

SSS variability with spatial scales smaller than ~ 150-km footprint can contribute to differences between satellite and in-situ measurements. Such small-scale horizontal variations can occur at fronts and eddies. Drucker and Riser (2014) noted that the influence of the horizontal variation within a footprint was larger than the vertical variation. Vinogradova and Ponte (2013) found that in a 1°x1° region (which approximates the size of the Aquarius footprint) the rmsd of daily SSS values computed with a 1/12°-grid model constrained with observations was typically less than 0.1 psu, but were greater than 0.2 psu near strong currents (e.g., Gulf Stream, Kuroshio, and Agulhus), outflows of major rivers (e.g., Amazon and Congo), and coastal regions (e.g., Gulf of Alaska and Arctic Ocean).

Reagan et al. (2014) noted that Aquarius SSS was up to 0.1 psu lower in the 10°S-20°N region than a composite of in-situ SSS data measured with ships, buoys and floats; poleward of these latitudes, Aquarius measured larger SSS values compared to in-situ measurements. Apparently, it is very challenging for Aquarius and SMOS to meet their pre-launch goals at latitudes higher than ~ 40° because cold surface water reduces the sensitivity of a L-band radiometer on SSS (Boutin et al., 2012; Lagerloef et al., 2013). Also, high wind (Font et al., 2013; Lagerloef et al., 2008) and sea ice reduce the accuracy of SSS retrievals (Reagan et al., 2014) due to difficulties in modeling these geophysical effects. Also, SSS retrievals in the coastal zone (especially near large populations) were less accurate than over the open ocean. Human-induced radio frequency interference cause low SSS retrievals even though both Aquarius and SMOS operate in the protected L-band spectrum of 1.400-1.4.27 GHz (Askoy and Johnson, 2013). This error is mostly restricted to the Northern Hemisphere regions in the northeast Atlantic near Europe, northwest Atlantic near Canada and the United States, and northwest Pacific near China and Japan (Reagan et al. 2014).

3 RESULTS

Evidence of the quality of a new data product, such as Aquarius and SMOS SSS, is acquired through replication of known phenomenon with additional insight provided by the new observations. Several examples are described.

3.1 Global Hydrological Balance

Wust (1936; see Sverdrup et al., 1942) was the first to notice the essential linkage between SSS and evaporation minus precipitation (E-P), in which the global patterns are illustrated in Figure 1c. Comparing Figure 1a or 1b with Figure 1c, regions with

positive (negative) E-P are correlated with high (low) SSS. When the E-P difference at the sea surface is greater (less) than zero, the SSS will increase (decrease) when other influences on SSS are constant. Formation and melt of sea ice produce effects on SSS similar to E-P. High SSS occurs in subtropical latitudes with the sinking dry air masses of the Hadley Circulation causing increased evaporation by the trade wind. Low SSS occurs in high latitudes where storms frequently occur and in the tropical zones with high rainfall such as the Intertropical Convergence Zone (ITCZ) and South Pacific Convergence Zone.

The North Atlantic Ocean has the global maximum open-ocean SSS (Figures 1a and 1b) because most of the basin is under the direct influence of the dry surface trade wind. The strength of E-P > 0 between 10 °N, where SSS is low because of rainfall in the ITCZ, and 25 °N, where SSS is maximum, illustrates the influence of the northwest Ekman surface current and northeast trade wind (Bingham et al., 2014). Gordon and Giulivi (2014) indicate that eddies are important in the northward transport of fresh surface water. When the surface water reaches ~ 25 °N, the northward current component diminishes to zero because the Ekman transport becomes balanced by the southward geostrophic current (Bingham et al., 2014). The absence of a SSS annual cycle between 20 °N and 30°N (Figure 2) is remarkable considering all other atmosphere and ocean variables have annual cycles at 25 °N. Understanding the SSS maximum within the global integrated Earth system has become a first-order challenge (Dohan et al., 2015; Dong et al., 2015; Schmitt et al., 2015).

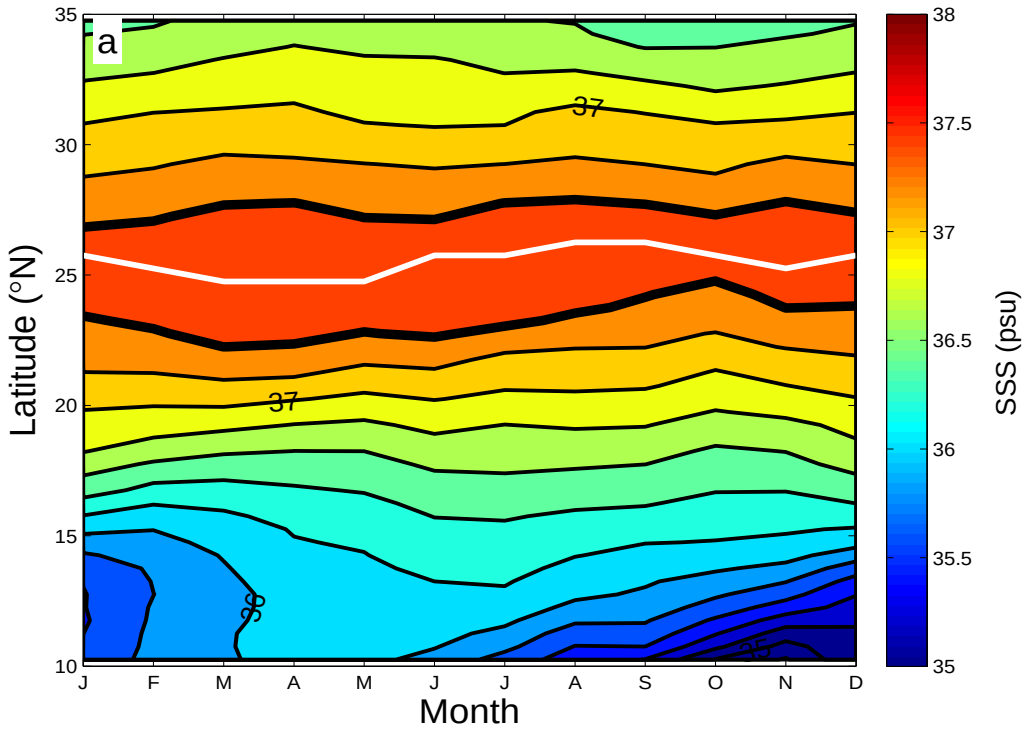

Figure 2. Monthly averaged Aquarius SSS recorded between 45 °W and 30 °W as a function of latitude from 10 °N to 35 °N for August 2011 to September 2013. Contour interval is 0.2 psu. White line is the latitude of maximum SSS for each month. Heavy line is an arbitrarily chosen value of 37.4 psu. Diagram extracted from Bingham et al. (2014).

Durack (2015) showed a strengthening of the hydrological cycle with ocean areas having high (low) SSS becoming more (less) saltier (Figure 3). Durack et al. (2012) indicated that a global warming of 1 °C would increase the global hydrological cycle by ~ 8 %. Wet areas dominated by precipitation would become wetter and dry areas dominated by evaporation would become drier (Held and Soden, 2006).

The availability of Aquarius and SMOS data triggered development of new analyses of oceanic behavior to improve physical parameterization of freshwater flux in coupled ocean-atmosphere models for studies of the global water cycle (Nieves et al., 2014).

3.2 Ocean Circulation

3.2.1 Tropical Instability Waves

Legeckis (1977) used satellite SST measurements to observe westward-propagating waves with a zonal wavelength of about 1100 km along the northern SST front between the cold-water tongue and warmer water in satellite SST measurements. Halpern et al. (1988) used moored current measurements at and near the Pacific

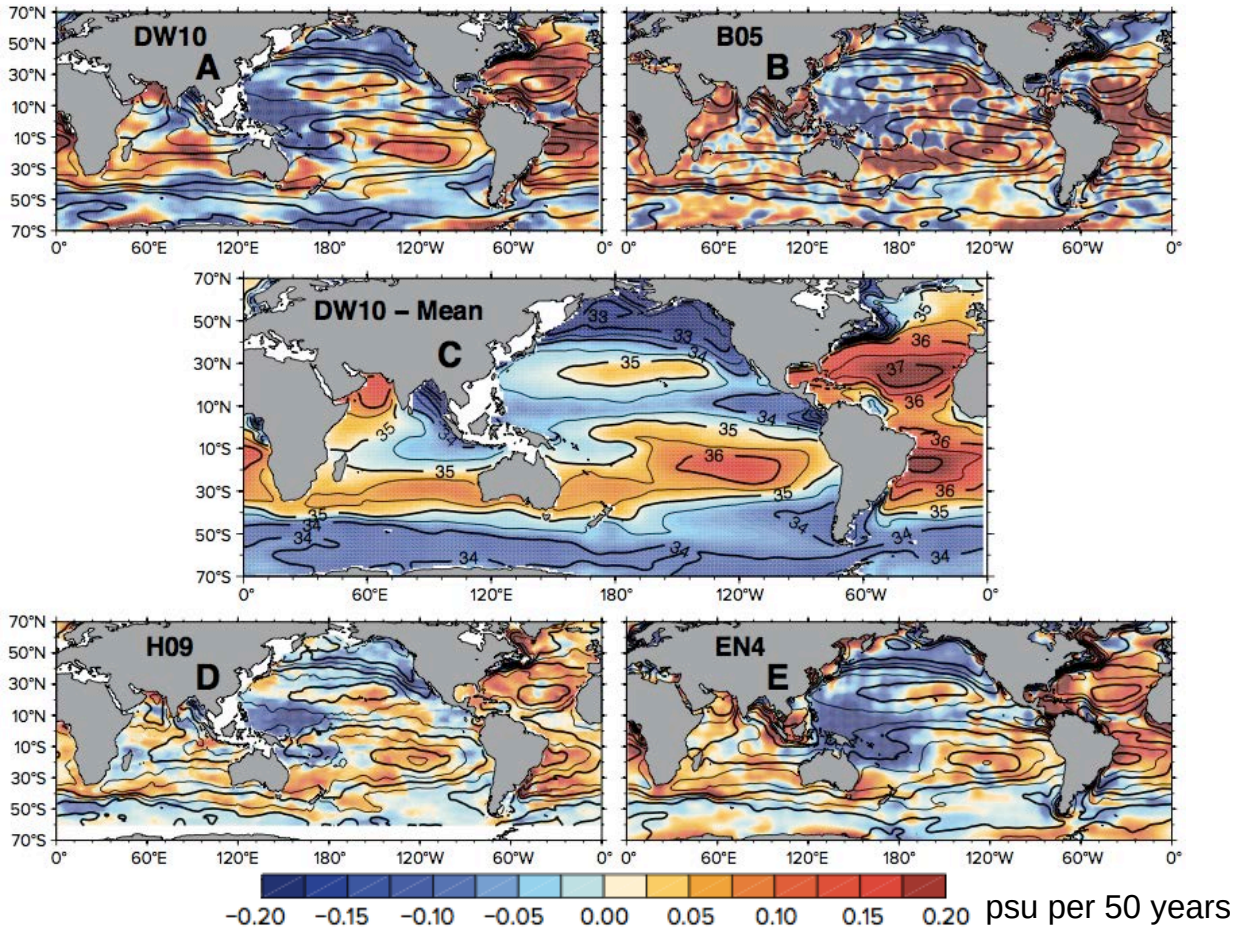

Figure 3. (A), (B), (D) and (E) are four different representations of the observed 50-year trend in SSS compiled by Durack (2015), and (C) the mean salinity distribution associated with (A). Diagram extracted from Durack (2015).

equator to show the long waves had characteristics of mixed Rossby-gravity waves, which propagated westward with a period of about 20 days, zonal wavelength of 1400 km and phase speed of about 85 cm s^{-1}, had large meridional current speed and near-zero zonal current speed, and were seasonally and inter-annually modulated with minimum (maximum) strength in March-May (September-November) and in an El Niño (La Niña) event. In addition to SST and current measurements, ocean color measurements of chlorophyll also show long waves with features similar to those observed with SST and ocean velocity (Strutton et al., 2001). These waves are also known as tropical instability waves (TIW) because the origin is barotropic instability between the westward-flowing South Equatorial Current and the eastward-flowing North Equatorial Countercurrent. Most of the mesoscale variability in tropical regions is associated with TIWs in contrast to the intense small-scale eddies and rings prevalent throughout the mid-latitude ocean (Chelton et al., 2011).

Lee et al. (2012) found that Aquarius SSS variations associated with TIWs at the equator of the Pacific Ocean have a dominant period of 17 days (Figure 4), in contrast to TIWs a few degrees of latitude to the north where the dominant period was 33 days. Moreover, they found that the 17-day period TIWs propagated at about 1 m s^{-1}, which was nearly twice as fast as the 33-day period TIWs. Also, Yin et al. (2014) detected the same two TIW features in an analysis of SMOS SSS data. Yin et al. (2014) noted that the 33-day TIW was not associated with the classical TIW description with a strong meridional current oscillation at the equator (Philander et al., 1985; Halpern et al., 1988). The TIW is known to occur in the Atlantic Ocean (Chelton et al., 2000), which has a similar type of current structure near the equator

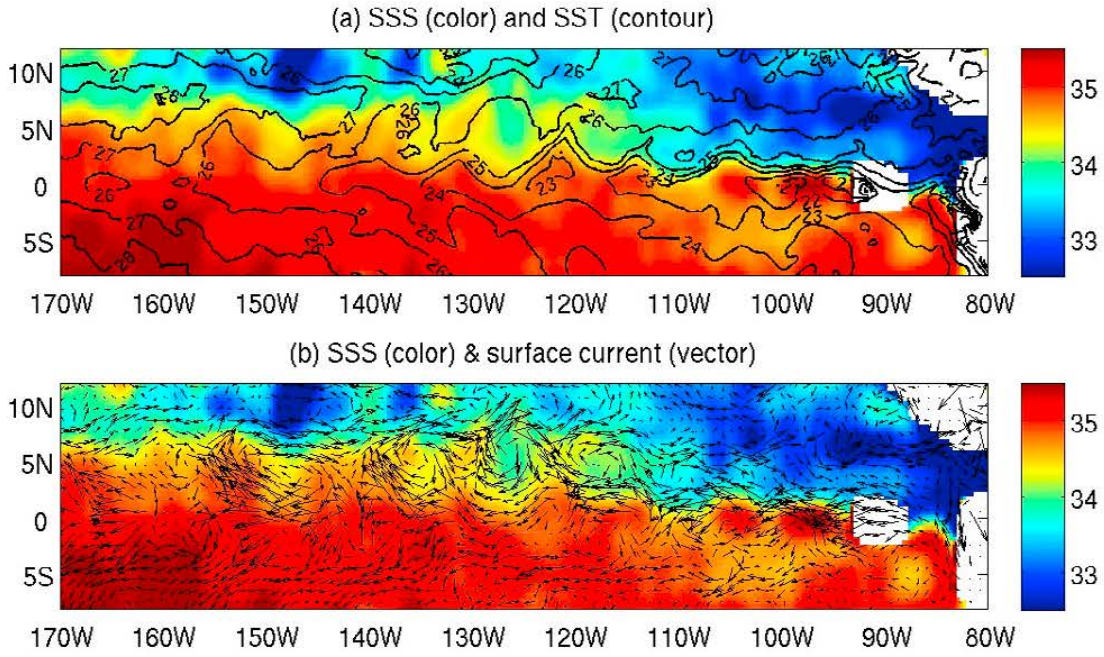

Figure 4. (a) Seven-day averaged SST (°C; represented by contours) and Aquarius SSS (psu; represented by colors). (b) Seven-day averaged SSS (psu; represented by colors) and 10-day averaged current vectors. Time intervals were centered on 18 December 2011. Diagram extracted from Lee et al. (2012).

as in the Pacific but the SSS front has a greater northeast-southwest slope, which is quite different that the zonal SST front at ~ 2N over the eastern two-thirds of the equatorial basin. Lee et al. (2014) used Aquarius SSS data to capture TIWs with an approximate 35-day (actually 20-50 days) period, westward speed of ~ 0.5 m s^{-1}, 1100-km zonal wavelength, and seasonal variability of TIWs, including the additional feature that SSS regulated the seasonal onset of TIWs because the TIW observed with SSS occurred earlier by about 1 month than the TIW recorded with SST. Lee et al. (2014) also found that the surface eddy perturbation potential energy associated with TIWs estimated from SSS and SST was three times larger than that estimated with only SST data. The SSS-dependent characteristics could improve understanding of the baroclinic-barotrophic origin of TIWs.

3.2.2 Rossby Waves

Subrahmanyam et al. (2009) detected an annual westward-propagating Rossby wave in the South Indian Ocean in satellite sea surface topography and numerical model simulations. Menezes et al. (2014) analyzed two years of Aquarius SSS and five years of Argo 5-m salinity data and found a significant annual feature at 20 °S between the Mid-Indian Ridge and the Ninety East Ridge in the central South Indian Ocean propagating towards the southwest at ~ 20 cm s^{-1} (Figure 5) with characteristics of a Rossby wave, which contained ~ 92 % of the annual variance.

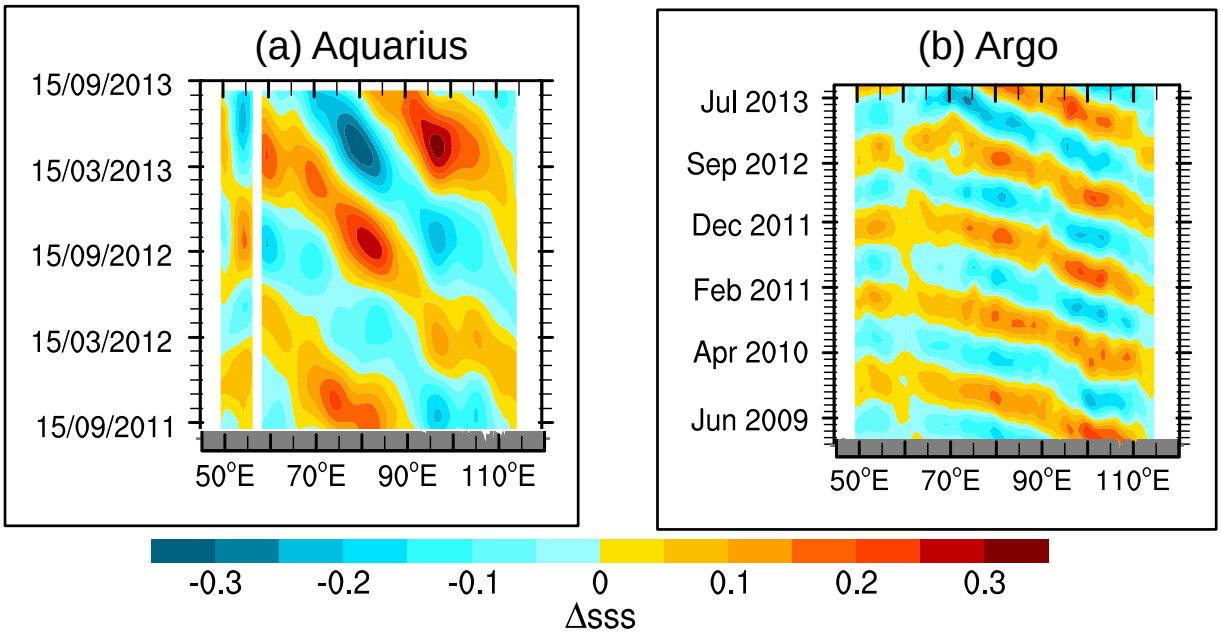

Figure 5. Annual Rossby wave detected in (a) Aquarius and (b) Argo data. Diagram produced from Figures 9(b) and 10(b) in Menezes et al. (2014).

3.2.3 Riverine Outflow: A Passive Tracer of Ocean Currents

In some regions near the coast, low SSS occurs in response to river outflow of freshwater and, sometimes, the impact of riverine water can be observed hundreds of kilometers from the coast. For example, Gierach et al. (2013) detected the effects of Mississippi River discharge into the Gulf of Mexico. Aquarius and SMOS data recorded Amazon River water entrained in the eastward-flowing North Equatorial

Countercurrent (Figures 1a and 1b; Reul et al. (2014a)). The SSS in the East China Sea is strongly correlated with Yangtze River discharge (Kim et al., 2014). However, other factors also need to be considered, such as intrusion of open ocean water regulating coastal SSS. For example, in the South China Sea in 2012 the riverine waters from the Mekong and Pearl Rivers had a negligible impact on Aquarius SSS compared to a substantially reduced flow of the Kuroshio (Zeng et al., 2014).

The combined Amazon and Orinoco plume adds a 1-m freshwater lens to inhibit near-surface vertical mixing, which increases SST to strengthen hurricane intensity when a hurricane moves through the region (Balaguru et al., 2012; Grodsky et al., 2012). Also, the salinity barrier layer weakens the reduction in SST produced by a hurricane. Therefore, SSS data should be included in forecasting hurricanes in the northwest Atlantic Ocean.

The confluence zone of the southward-flowing Brazil Current and northward-flowing Malvinas is a choice location to use SSS to study the interleaving of water masses because of the very large SSS gradient produced by the Brazil Current with SSS of ~ 36 psu and Malvinas Current with SSS of ~ 34 psu. Aquarius detected freshwater discharge from the Rio de al Plata and nearby lagoons (Figure 6a). Matano et al. (2014) concluded with analysis of model simulations that Aquarius variations represented two-dimensional mass exchange from the continental shelf to the deep ocean, with an associated 1.2 Sv flow onto and out of the shelf (Figure 6b).

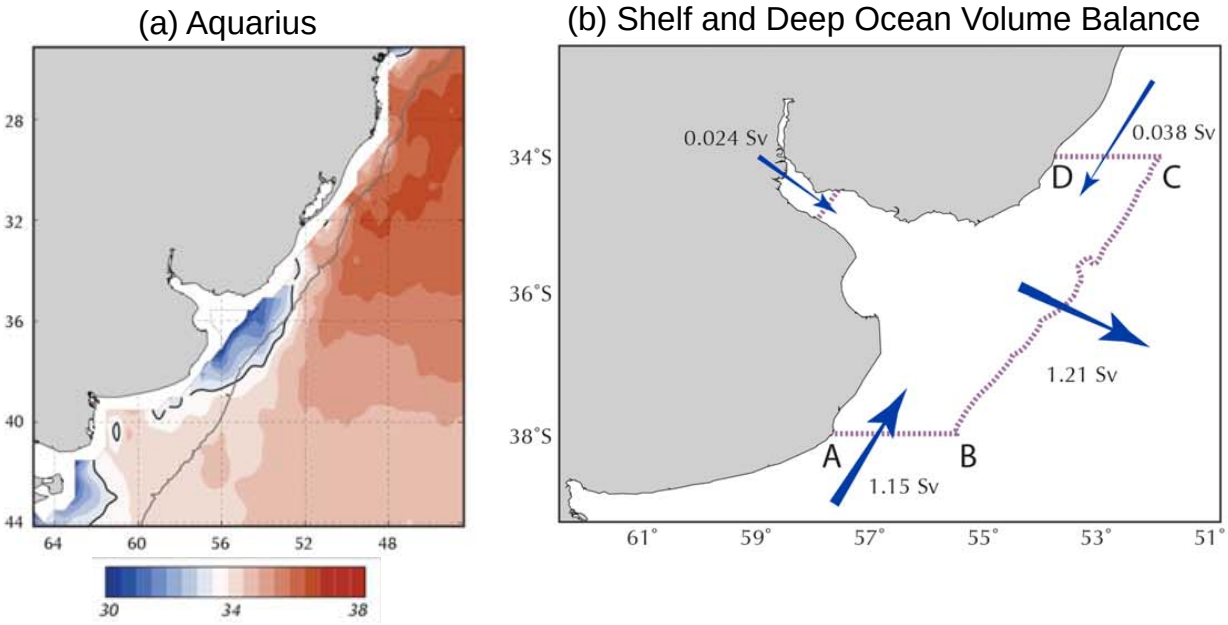

Figure 6. Water mass balance at Brazil-Malvinas Current Confluence Zone (a) Aquarius SSS distribution and (b) alongshore and offshore transports. Diagram produced from Figures 10 and 14(a) in Matano et al. (2014).

3.2.4 Mesoscale Motions

Mesoscale motions with horizontal scales of about 10-100 km and time scales of 2-50 days, including rings and meanders, are ubiquitous throughout the mid-latitude ocean, e.g., see Figure 5 in Halpern and Fu (2013). Mesoscale features are typically

observed in satellite SST measurements when appropriate SST gradients occur. On some occasions when the SST gradient is not well established, perhaps because of summer conditions, SSS gradients may be large enough to recognize mesoscale motions. Such conditions occur in the Gulf Stream region in summer months. Reul et al. (2014b) found SMOS SSS data provided critical evidence for monitoring Gulf Stream meanders and rings (Figure 7). Aquarius and SMOS SSS data both yielded similar measurements of Gulf Stream cold-core rings (Umbert et al., 2015), which were not visible in SST imagery.

Kolodziejczyk et al. (2015) showed that SMOS could identify SSS mesoscale structures near the Azores Front with comparable spatial resolution of SST and ocean color measurements.

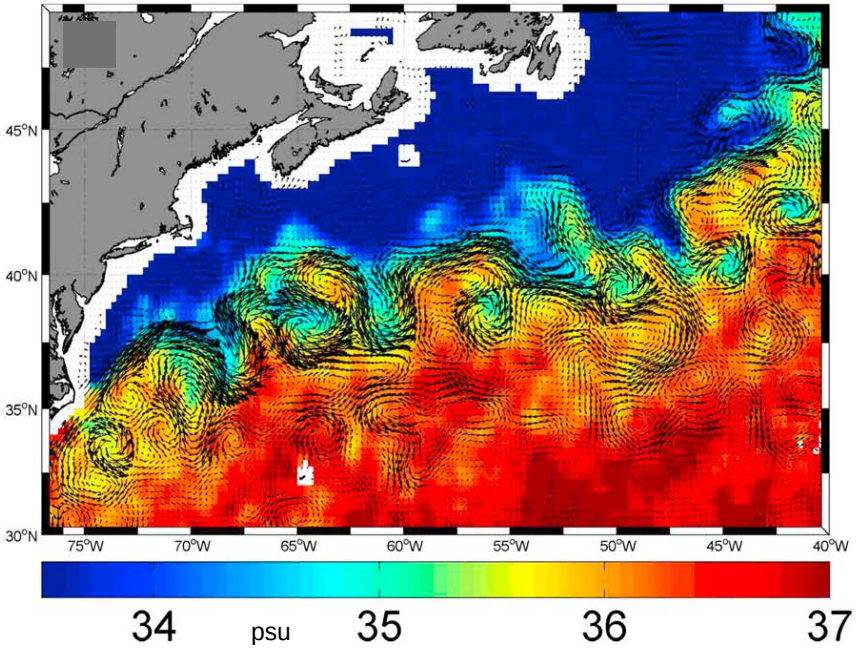

Figure 7. SMOS SSS averaged from 15-25 August 2012. Arrows represent OSCAR surface current. Diagram extracted from Reul et al. (2014b).

3.3 El Niño and La Niña

An El Niño (La Niña) occurs when the monthly SST anomaly (SSTA) or difference from a 30-year mean in the Niño 3.4 region (5°S-5°N, 170°W-120°W) is above (below) 0.5 °C for five consecutive months, when each month represents a 3-month average SST (http://www.cpc.ncep.noaa.gov/products/analysis_monitoring/ensostuff/ensoyears.shtml). We arbitrarily classify the strength of an El Niño and La Niña event as weak when the maximum SSTA was |0.5 – 1.0| °C, as moderate when maximum SSTA was |1.0 – 1.5| °C, as strong when the maximum SSTA was |1.5 – 2.0| °C, and as intense when the maximum SSTA was greater than |2.5| °C. The SMOS mission began when a strong El Niño event was occurring; the event began in July 2009 and continued until April 2010. SMOS also observed the moderate La Niña event of July 2010 to April 2011 before the launch of Aquarius. Both Aquarius and SMOS recorded SSS in the moderate La Niña event of September 2011 to March 2012.

This La Niña event was followed by 30 normal months, when a weak El Niño event began in October 2014.

Lukas and Lindstrom (1991) noted that salinity stratification could modulate air-sea interactions in the west Pacific warm pool during an El Niño event. Zhu et al. (2014) showed that near-surface salinity variability in the equatorial Pacific would influence the tendency for onset and maintenance of El Niño conditions because of the salinity effect on stratification and horizontal pressure gradient. Delcroix (1998) found that the El Niño/La Niña variation of SSS was mainly located in the west Pacific where the 1.0 psu SSS difference between El Niño and La Niña was twice as large as the peak-to-trough variation in the seasonal cycle. Unfortunately, from the perspective of mitigating the influence of TIWs on sampling SSS during El Niño/La Niña, the 17-day period TIW SSS crest-to-trough difference was also ~ 1.0 psu and 0.5 psu for the 33-day period TIWs and about half the magnitude for 17-day period TIW (Yin et al., 2014); fortunately, TIW amplitudes are three times greater in the east Pacific at 0°, 140°W than in the west Pacific at 0°, 150°E (Halpern, 1989). Thus, TIWs are not expected to impact the interpretation of SSS in the west Pacific, where an El Niño event would originate.

Hasson et al. (2014), in a comparison of the July 2010 (the first month of a La Niña event when the ONI was - 0.9 °C) and July 2011 (when the ONI had a normal value of - 0.2) SMOS SSS distributions in the west Pacific warm pool, observed that the SSS along the equator from 150°E to 170°E was approximately 0.4 psu higher during La Niña compared normal conditions (Figure 8). Higher SSS would be expected to be associated with lower rainfall.

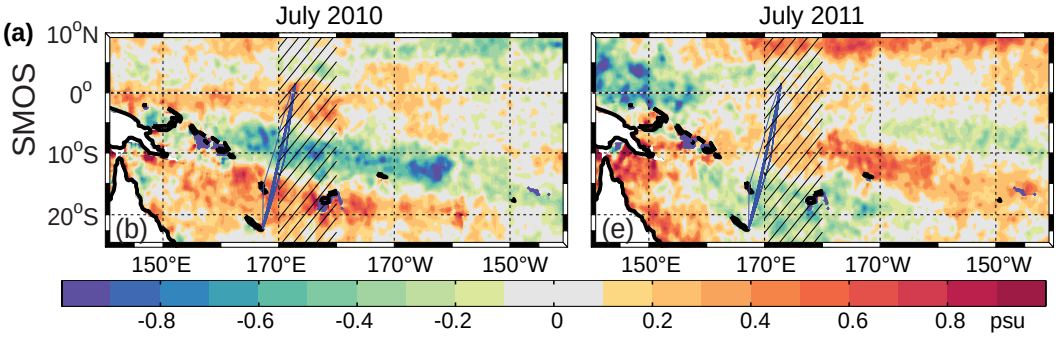

(b)

Year	DJF	JFM	FMA	MAM	AMJ	MJJ	JJA	JAS	ASO	SON	OND	NDJ
2000	-1.7	-1.5	-1.2	-0.9	-0.8	-0.7	-0.6	-0.5	-0.6	-0.6	-0.8	-0.8
2001	-0.7	-0.6	-0.5	-0.4	-0.2	-0.1	0.0	0.0	-0.1	-0.2	-0.3	-0.3
2002	-0.2	0.0	0.1	0.3	0.5	0.7	0.8	0.8	0.9	1.2	1.3	1.3
2003	1.1	0.8	0.4	0.0	-0.2	-0.1	0.2	0.4	0.4	0.4	0.4	0.3
2004	0.3	0.2	0.1	0.1	0.2	0.3	0.5	0.7	0.8	0.7	0.7	0.7
2005	0.6	0.4	0.3	0.3	0.3	0.3	0.2	0.1	0.0	-0.2	-0.5	-0.8
2006	-0.9	-0.7	-0.5	-0.3	0.0	0.1	0.2	0.3	0.5	0.8	1.0	1.0
2007	0.7	0.3	-0.1	-0.2	-0.3	-0.3	-0.4	-0.6	-0.8	-1.1	-1.2	-1.4
2008	-1.5	-1.5	-1.2	-0.9	-0.7	-0.5	-0.3	-0.2	-0.1	-0.2	-0.5	-0.7
2009	-0.8	-0.7	-0.5	-0.2	0.2	0.4	0.5	0.6	0.8	1.1	1.4	1.6
2010	1.6	1.3	1.0	0.6	0.1	-0.4	-0.9	-1.2	-1.4	-1.5	-1.5	-1.5
2011	-1.4	-1.2	-0.9	-0.6	-0.3	-0.2	-0.2	-0.4	-0.6	-0.8	-1.0	-1.0
2012	-0.9	-0.6	-0.5	-0.3	-0.2	0.0	0.1	0.4	0.5	0.6	0.2	-0.3
2013	-0.6	-0.6	-0.4	-0.2	-0.2	-0.3	-0.3	-0.3	-0.3	-0.2	-0.3	-0.4
2014	-0.6	-0.6	-0.5	-0.1	0.1	0.1	0.0	0.0	0.2	0.5	0.7	0.7
2015	0.6	0.5										

Figure 8. (a) SMOS SSS measurements in the west Pacific warm pool in July 2010 (La Niña conditions) and July 2011 (normal conditions). Diagram extracted from Hasson et al. (2014). (b) NOAA Oceanic Niño Index for Nino 3.4 region.

A coupled ocean and atmosphere model constrained with observations is the foundation of many forecasts of El Niño and La Niña events. Hackert et al. (2014) showed that the monthly forecast skill for SST anomaly in the Nino 3 region (5°S-5°N, 150°W-90°W) in August 2011 to February 2014 improved considerably with assimilation of Aquarius SSS, e.g., for forecast lead times greater than 5 months, the correlation coefficient and rmsd between the modeled and observed SSTA was 2.5 times larger and 40% smaller, respectively. Assimilation of only in-situ salinity measurements recorded within the uppermost 10 m provided less accurate forecasts of Niño 3 SST anomaly. Hackert et al. (2014) conjectured that many of the incorrect forecasts of the El Niño event for late 2012 were due to the inadequate observational constraint of SSS in the forecast model near the equator.

Satellite SSS data have bias difference and rmsd compared with in-situ data, which need to be mitigated before their assimilation in models. Vernieres et al. (2014) developed a neural network method that reduced bias and rmsd errors in Aquarius SSS data. Assimilation of SMOS SSS data into a numerical model of the northeast subtropical Atlantic Ocean has shown the potentiality of satellite SSS observations to provide coherent salinity maps (Hoareau et al., 2014).

4 SUMMARY AND CONCLUSIONS

The Aquarius and SMOS Missions demonstrated the feasibility of L-band technology to measure SSS with adequate accuracy and precision for generation of new knowledge about ocean circulation and dynamics. The oceanographic community has reinvigorated the study of salinity. Familiar science results have been replicated and new knowledge has been generated.

Before the launch of the Aquarius and SMOS missions, knowledge of SSS variability was severely hampered by an absence of long-term datasets, especially those over a region. Analyses of satellite SSS with in-situ salinity measurements have increased understanding of TIWs and Rossby waves. Closing the salt budget in select regions, such as in the North Atlantic high SSS zone, represent a beginning in narrowing the uncertainties in the marine hydrological cycle. Analysis of the salt budget in a rainfall region is under consideration in 2016-2017 in the eastern tropical Pacific (SPURS-2 Planning Group, 2015). The global salt budget would remain a challenge until the L-band sensitivity to low SST is somehow reduced. An improvement in forecasting El Niño/La Niña through consideration of SSS seems doable. Also, satellite SSS data have the potential to increase knowledge of biogeochemical processes, such as ocean acidification (Land et al., 2015).

Recommendations by the CLIVAR Salinity Working Group (2008) for satellite SSS observations are current today. As described above, salinity measured with Argo floats, salinity instruments on ships-of-opportunity and research vessels, gliders, and moored buoys are critical data sources to merge with satellite SSS. Aquarius and SMOS data are ripe for integration and assimilation into coupled ocean-atmosphere general circulation models. An intriguing suggestion to explore is that SSS would have shorter horizontal scales of variability compared to SST because SSS has no direct exchange with the atmosphere unlike SST, in which the atmosphere would

tend to smooth lateral variations in SST. Analyses of SSS and its contribution to upper-ocean mixing and interaction with Ekman advection, especially at outcropping isopycnals, is a challenging problem.

5 ACKNOWLEDGEMENTS

We are grateful to Dr. Tong Lee (Jet Propulsion Laboratory) and Dr. Stephanie Guinehut (Collecte Localisation Satellites) for perceptive comments on a preliminary draft version. DH is indebted to Jack Kaye (NASA Headquarters) for his support for participation in CGMS. Part of this research was carried out at the Jet Propulsion Laboratory, California Institute of Technology, under a contract with the National Aeronautics and Space Administration.

6 REFERENCES

Abe, H. and N. Ebuchi (2014) Evaluation of sea-surface salinity observed by Aquarius. *Journal of Geophysical Research Oceans*, *119*, 8109-8121, doi:10.1002/2014JC010094.

Askoy, M. and J. T. Johnson (2013) A comparative analysis of low-level radio frequency interference in SMOS and Aquarius Microwave radiometer measurements. *IEEE Transactions on Geoscience and Remote Sensing*, *51*, 4983-4992, doi: 10.1109/TGRS.2013.2266278.

Balaguru, K., P. Chang, R. Saravanan, L. R. Leung, Z. Xu, M. Li and J.-S. Hsieh (2012) Ocean barrier layers' effect on tropical cyclone intensification. *Proceedings of the National Academy of Sciences*, *109*, 14343-14347, doi:10.1073/pnas.1201364109.

Bingham, F. M., J. Busecke, A. L. Gordon, C. Giulivi and Z. Li (2014) The North Atlantic subtropical surface salinity maximum as observed by Aquarius. *Journal of Geophysical Research Oceans*, *119*, 7741-7755, doi:10.1002/2014JC009825.

Boutin, J., N. Martin, X. Jin, J. Font, N. Reul and P. Spurgeon (2012) First assessment of SMOS data over open ocean: Part II – Sea surface salinity. *IEEE Transactions on Geoscience and Remote Sensing*, *50*, 1662-1675.

Chelton, D. B., M. G. Schlax and R. M. Samelson (2011) Global observations of nonlinear mesoscale eddies. *Progress in Oceanography*, *91*, 167-216.

Chelton, D. B., F. J. Wentz, C. L. Gentemann, R. A. de Szoeke and M. G. Schlax (2000) Satellite microwave SST observations of transequatorial tropical instability waves. *Geophysical Research Letters*, *27*, 1239-1242.

CLIVAR Salinity Working Group (2008) What's next for salinity? *Oceanography*, *21*, 82-86.

Delcroix, T. (1998) Observed surface oceanic and atmospheric variability in the tropical Pacific at seasonal and ENSO timescales: A tentative overview. *Journal of Geophysical Research*, *103*, 18611-18633, doi:10.1029/98JC00814.

Dohan, K., H.-Y. Kao and G.S.E. Lagerloef (2015) The freshwater balance over the North Atlantic SPURS domain from Aquarius satellite salinity. *Oceanography, 28*, 86–95, http://dx.doi.org/10.5670/oceanog.2015.07.

Dong, S., G. Goni and R. Lumpkin (2015) Mixed-layer salinity budget in the SPURS region on seasonal to interannual time scales. *Oceanography*, *28*, 78–85, http://dx.doi.org/10.5670/oceanog.2015.05.

Drucker, P. J. and S. C. Riser (2014) Validation of Aquarius sea surface salinity with Argo: Analysis of error due to depth of measurement and vertical salinity stratification. *Journal of Geophysical Research Oceans*, *119*, 4626-4637, doi:10.1002/2014JC010045.

Durack, P. J. (2015) Ocean salinity and the global water cycle. *Oceanography* 28, 20–31, http://dx.doi.org/10.5670/oceanog.2015.03.

Durack, P. J., S. E. Wijffels and R. J. Matear (2012) Ocean salinities reveal strong global water cycle intensification during 1950 to 2000. *Science*, *336*, 455-458, doi:10.1126/science.1212222.

Font, J., J. Boutin, N. Reul, P. Spurgeon, J. Ballabrera-Poy, A. Chuprin, C. Gabarró, J.Gourrion, S. Guimbard, C. Hénocq, S. Lavender, N. Martin, M. McCuloch, I. Meirold-Mautner, C. Mugerin, F. Petitcolin, M. Portabella, R. Sabia, M. Talone, J. Tenerelli, A. Turiel, J. L. Vergely, P. Waldteufel, X. Yin, S. Zine and S, Delwart (2013) SMOS first data analysis for sea surface salinity determination. *International Journal of Remote Sensing*, *34*, 3654-3670, doi:10.1080/01431161.2012.716541.

Font, J., A. Camps, A. Borges, M. Martin-Neira, J. Boutin, N. Rueul, Y. Kerr, A Hahne and S. Mecklenburg (2010) SMOS: The Challenging measurement of sea surface salinity from space. *Proceedings of the IEEE*, *98*, 649-665.

Gierach, M. M., J. Vazquez, T. Lee and V. Tsontos (2013) Aquarius and SMOS detect effects of an extreme Mississippi River flooding event in the Gulf of Mexico. *Geophysical Research Letters*, *40*, doi:10.1002/grl50995.

Gordon, A. L. and C. F. Giulivi (2014) Ocean eddy freshwater flux convergence into the North Atlantic subtropics. *Journal of Geophysical Research Oceans*, *119*, 3327-3335, doi:10.1002/2013JC009596.

Grodsky, S. A., N. Reul, G. Lagerloef, G. Reverdin, J. A. Carton, B. Chapron, Y. Quilfen, V. N. Kudryavtsev and H.Y. Kao (2012) Haline hurricane wake in the Amazon/Orinoco plume: Aquarius/SADD and SMOS observations. *Geophysical Research Letters*, *39*, doi:10.1029/2012GL053335.

Hackert, E., A. J. Busalacchi and J. Ballabrera-Poy (2014) Impact of Aquarius sea surface salinity observations on coupled forecasts for the Indo-Pacific Ocean. *Journal of Geophysical Research Oceans*, *119*, 4045-4067, doi:10.1002/2013JC009697.

Halpern, D. (1989) Detection of 17.5-day period meridional current oscillations in the equatorial western Pacific Ocean during 1985. *Geophysical Research Letters*, *16*, 499-502.

Halpern, D. and L.-L. Fu (2013) Satellite global ocean surface topography measurements: Challenges and Opportunities. CGMS-41 IOC-WP-01, 14 pp.

Halpern, D., G. Lagerloef and J. Font (2012) Sea surface salinity: Research challenges and opportunities. Coordination Group for Meteorological Satellites, CGMS-40 NASA-WP-04, 7 pp.

Halpern, D., R. A. Knox and D. S. Luther (1988) Observations of 20-day period meridional current oscillations in the upper ocean along the Pacific equator. *Journal of Physical Oceanography*, *18*, 1514-1534.

Hasson, A., T. Delcroix, J. Boutin, R. Dussin and J. Ballabrera-Poy (2014) Analyzing the 2010-2011 La Nina signature in the tropical pacific sea surface salinity using in situ data, SMOS observations, and a numerical simulation. *Journal of Geophysical Research Oceans*, *119*, 3855-3867, doi:10.1002/2013JC009388.

Held, I. M. and B. J. Soden (2006) Robust responses of the hydrological cycle to global warming. *Journal of Climate*, *19*, 5686-5699, doi:10.1175/JCL13990.1.

Henocq, C., J. Boutin, F. Petitcolin, G. Reverdin, S. Arnault and P. Lattes (2010) Vertical variability of near-surface salinity in the tropics: Consequences for L-band radiometer calibration and validation. *Journal of Atmospheric and Oceanic Technology*, *27*, 192-209, doi:10.1175/2009JTECHO670.1.

Hoareau, C., M. Umbert, J. Martínez, A. Turiel and J. Ballabrera-Poy (2014) On the potential of data assimilation to generate SMOS-Level 4 maps of sea surface salinity. *Remote Sensing of Environment*, *146*, 188-200, doi:1016/J.RES.2013.10.005.

Kim, S., J. H. Lee, P. de Mattha, S. Yueh, C.-S. Hong, J.-H. Lee and G. Lagerloef (2014) Sea surface salinity variability in the East China Sea observed by the Aquarius instrument. *Journal of Geophysical Research Oceans*, *119*, 7016-7028, doi:10.1002/2014JC009983.

Kolodziejczyk, N., O. Hernandez, J. Boutin and G. Reverdin (2015) SMOS salinity in the subtropical North Atlantic salinity maximum: 2. Two-dimensional horizontal thermohaline variability. *Journal of Geophysical Oceans*, *120*, 972-987, doi:10.1002/2014JC010103.

Lagerloef, G., H.-K. Kao, O. Melnichenko, P. Hacker, E. Hackert, Y. Chao, K. Hilburn, T. Meissner, S. Yueh, L. Hong and T. Lee (2013) Aquarius salinity validation

analysis, data version 2.0. Aquarius Project Document AQ-014-PS-0016 (18 February 2013).

Lagerloef, G., F. Wentz, S. Yueh, H.-Y. Kao, G. C. Johnson and J. M. Lyman (2012) Aquarius satellite mission provides new, detailed view of sea surface salinity in "State of the Climate in 2011." *Bulletin of the American Meteorological Society*, *93*, S70-S71.

Lagerloef, G. and J. Font (2010) SMOS and Aquarius/SAC-D missions: The era of spaceborne salinity measurements is about to begin. In, *Oceanography From Space*, V. Barale et al., Eds. Springer, 35-58 pp.

Lagerloef, G., F. R. Colomb, D. Le Vine, F. Wentz, S. Yueh, C. Ruf, J. Lilly, J. Gunn, Y. Chao, A. deCharon, G. Feldman and C. Swift (2008) The Aquarius/SAC-D mission: Designed to meet the salinity remote-sensing challenge. *Oceanography*, *21*, 68-81.

Land, P. E., J. D. Shutler, H. Findlay, F. Girard-Ardhuin, R. Sabia, N. Reul, J. F. Piolle, B. Chapron, Y. Quikfen, J. E. Salisbury, D. Vandemark, R. Bellerby and P. Bhadury (2015) Salinity from space unlocks satellite-based assessment of ocean acidification. *Environmental Science and Technology*, *49*, 1987-1994, doi:10.1021/es504849s.

Lee, T., G. Lagerloef, H.-Y. Kao, M. J. McPhaden, J. Willis and M. M. Gierach (2014) The influence of salinity on tropical Atlantic instability waves. *Journal of Geophysical Research Oceans*, *119*, doi:10.1002/2014JC010100.

Lee, T., G. Lagerloef, M. M. Gierach, H.-Y. Kao, S. S. Yueh and K. Dohan (2012) Aquarius reveals salinity structure of tropical instability waves. *Geophysical Research Letters*, *39*, doi:10.1029/2012GL052232.

Legeckis, R. (1977) Long waves in the eastern equatorial Pacific Ocean: A view from a geostationary satellite. *Science*, *197*, 1179-1181.

Lukas, R.and E. Lindstrom (1991) The mixed layer of the western equatorial Pacific Ocean. *Journal of Geophysical Research*, *96*, 3343-3357.

Matano, R. P., V. Combes, A. R. Piola, R. Guerrero, E. D. Palma, P. T. Strub, C. James, H. Fenco, Y. Chao and M. Saraceno (2014) The salinity signature of the cross-shelf exchanges in the Southwestern Altantic Ocean: Numerical simulations. *Journal of Geophysical Research Oceans*, *119*, 7949-7968, doi:10.1002/2014JC010116.

Meissner, T., F. J. Wentz and L. Ricciardulli (2014) The emission and scattering of L-band microwave radiation from rough ocean surfaces and wind speed measurements from the Aquarius sensor. *Journal of Geophysical Research Oceans*, *119*, 6499-6522, doi: 10.1002/2014JC009837.

Menezes, V. V.,M. Vianna and H. E. Phillips (2014) Aquarius sea surface salinity in the South Indian Ocean: Revealing annual-period planetary waves. *Journal of Geophysical Research Oceans*, *119*, 3883-3980, doi:10.1002/2014JC009935.

Nieves, V., J. Wang and J. K. Willis (2014) A conceptual model of ocean freshwater flux derived from sea surface salinity. *Geophysical Research Letters*, *41*, 6452-6458, doi:10.1002/2014GL061365.

Philander, S. G. H., D. Halpern, R. Legeckis, L. Miller, C. Paul, R. Watts, R. Weisberg and M. Wimbush (1985) Long waves in the equatorial Pacific Ocean. *Transactions of the American Geophysical Union*, *66*, 154.

Reagan, J., T. Boyer, J. Antonov and M. Zweng (2014) Comparison analysis between Aquarius sea surface salinity and World Ocean Database in situ analyzed sea surface salinity. *Journal of Geophysical Research Oceans*, *119*, 8122-8140, doi:10.1002/2014JC009961.

Reul, N., S. Fournier, J. Boutin, O. Hernandez, C. Maes, B. Chapron, G. Alory, Y. Quilfen, J. Tenerelli, S. Morisset, Y. Kerr, S. Meckleburg, and S. Delwart (2014a) Sea surface salinity observations from space with the SMOS satellite: A new means to monitor the marine branch of the water cycle. *Surveys in Geophysics*, *35*, 681-722.

Reul, N., B. Chapron, T. Lee, C. Donlon, J. Boutin and G. Alory (2014b) Sea surface salinity structure of the meandering Gulf Stream revealed by SMOS sensor. *Geophysical Research Letters*, *41*, 3141-3148, doi: 10.1002/2014GL059215.

Riser, S. C., L. Ren and A. Wong (2008) Salinity in ARGO. *Oceanography*, *21*, 56-67.

Schmitt, R. W. and A. Blair (2015) A river of salt. *Oceanography*, *28*, 40–45, http://dx.doi.org/10.5670/oceanog.2015.04.

Schmitt, R. W., T. Boyer, G. Lagerloef, J. Schanze, S. Wijffels and L. Yu (2010). Salinity and the global water cycle. In: *Proceedings of OceanObs'09: Sustained Ocean Observations and Information for Society (Vol. 1),* Venice, Italy, 21-25 September 2009, Eds., Hall, J., D. E. Harrison and D. Stammer, ESA Publication WPP-306, doi:10.5270/OceanObs09.pp.34.

SPURS-2 Planning Group (2015) From salty to fresh—Salinity Processes in the Upper-ocean Regional Study-2 (SPURS-2): Diagnosing the physics of a rainfall-dominated salinity minimum. *Oceanography*, *28*, 150–159, http://dx.doi.org/10.5670/oceanog.2015.15.

Strutton, P. G., J. P. Ryan and F. P. Chavez (2001) Enhanced chlorophyll associated with tropical instability waves in the equatorial Pacific. *Geophysical Research Letters*, *28*, 2005-2008.

Subrahmanyam, B., D. M. Heffner, D. Cromwell and J. F. Shriver (2009) Detection of Rossby waves in multi-parameters in multi-mission satellite observations and

HYCOM simulations in the Indian Ocean. *Remote Sensing of the Environment*, *113*, 1293–1303, doi:10.1016/j.rse.2009.02.017.

Sverdrup, H. U, M. Johnson and R. Fleming (1942) *The Oceans: Their Physics, Chemistry and General Biology*. Prentice-Hall, Englewood, New Jersey, 1060 pp.

Umbert, M., S. Guimbard, G. Lagerloef, L. Thompson, M. Portabella, J. Ballabrera-Poy and A. Turiel (2015) Detecting the surface salinity signature of Gulf Stream cold-core rings in Aquarius synergistic products. *Journal of Geophysical Research Oceans*, *120*, 859-874, doi:10.1002/2014JC010466.

Vernieres, G., R. Kovach, C. Keppenne, S. Akella, L. Brucker and E. Dinnat (2014) The impact of the assimilation of Aquarius sea surface salinity data in the GEOS ocean data assimilation system. *Journal of Geophysical Research Oceans*, *119*, 6974-6987, doi:10.1002/2014JC010006.

Vinogradova, N. T. and R. M. Ponte (2013) Small-scale variability in sea surface salinity and implications for satellite-derived measurements. *Journal of Atmospheric and Oceanic Technology*, *30*, 2689-2694, doi:10.1175/JTECH-D-13-00110.1.

Yin, X., J. Boutin, G. Reverdin, T. Lee, S. Arnault and N. Martin (2014) SMOS sea surface salinity signals of tropical instability waves. *Journal of Geophysical Research Oceans*, *119*, 7811-7826, doi:10.1002/2014JC009960.

Yu, L. and R. A. Weller (2007) Objectively analyzed air-sea fluxes for the global ice-free oceans (1981-2005). *Bulletin of the American Meteorological Society*, *88*, 527-539.

Yueh, S. H., R. West, W. J. Wilson, F. K. Li, E. G. Njoku and Y. Rahmatsamii (2001) Error sources and feasibility for microwave remote sensing of ocean surface salinity. *IEEE Transactions on Geoscience and Remote Sensing*, *39*, 1049-1060.

Zeng, L., W. T. Liu, H. Xue, P. Xiu and D. Wang (2014) Freshening in the South China Sea during 2012 revealed by Aquarius and in situ data. *Journal of Geophysical Research Oceans*, *119*, doi:10.1002/2014JC010108.

Zhu, J., B. Huang, R.-H. Zhang, Z.-Z. Hu, A. Kumar, M. Balmaseda, L. Marx and J. L. Kinter III (2014) Salinity anomaly as a trigger for ENSO events. *Nature Scientific Reports*, *4*, Article Number 6821, doi:10.1038/srep06821.